

**Original Article** 

# A novel bath coagulation/electrospinning method to obtain crosslinked nanofibers based on calcium alginate and polyvinyl alcohol and In Vitro cytotoxicity evaluation

Innovador método de electrohilado/ baño de coagulación para obtener nanofibras entrecruzadas basadas en alginato de calcio y alcohol polivinilo y su evaluación citotóxica in vitro

Tonantzi Pérez-Moreno¹⊠ 💿 , M.J. Rivas-Arreola²⊠ 💿 , I. Santos-Sauceda³⊠ 💿 , R. Ramirez-Bon⁴⊠ 💿 , E.A. Elizalde-Peña¹

- Facultad de Ingeniería, Universidad Autónoma de Querétaro, Carr. A Chichimequillas S/N, Ejido Bolaños, 76140 Santiago de Querétaro, Qro., México.
- Departamento de Ciencias e Ingenierías, Universidad Iberoamericana Puebla, Blvd. Del Niño Poblano 2901, Reserva Territorial Atlixcáyotl, Centro Comercial Puebla, 72810 San Andrés Cholula, Pue., México.
- Departamento de Investigación en Polímeros y Materiales, Universidad de Sonora, Blvd. Luis Encinas J, Calle Av. Rosales &, Centro, 83000 Hermosillo, Son., México.
- Centro de Investigación y de Estudios Avanzados del IPN, Unidad Querétaro, Apdo, Postal 1-798, Querétaro, Qro., México.

# **ABSTRACT**

In tissue engineering, the availability of a scaffold is crucial; it must support cell growth, be biocompatible, and enable adequate perfusion of aqueous media. Although alginate is an approved polymer for biomedical applications, its processing to obtain membranes through electrospinning presents significant challenges. This work focuses on an efficient method to produce crosslinked nanofibers of alginate (NaAlg) and polyvinyl alcohol (PVA) using a coagulation bath with CaCl<sub>2</sub> during electrospinning, employing both single (SN) and coaxial (CN) needles. In the case of SN, the molar ratio was evaluated for the influence on fiber formation via electrospinning; meanwhile, for CN, the tip-to-collector distance was evaluated. Obtaining optimal conditions at 70 % NaAlg for SN, and 15 cm tip-to-collector distance for CN, both at a flow rate of 0.1 mL/h and a voltage of 19 kV. The resulting crosslinked nanofibers, with average diameters of  $70 \pm 17$  nm for SN and 124  $\pm$  20 nm for CN, displayed well-defined interconnected fibrous morphologies. The interactions between NaAlg and CaCl, were confirmed to be carboxylate calcium formation by FTIR. In vitro studies of CN NaAlg-PVA with JB6 fibroblast cells showed a cell proliferation rate of 124 %, demonstrating the substantial potential of these nanofibers for wound healing applications.

Keywords: Tissue engineering, skin wound, PVA/alginate nanofibers, coaxial electrospinning.

#### **RESUMEN**

Para la ingeniería de tejidos, es fundamental disponer de un andamio que soporte el crecimiento celular, sea biocompatible, y permita una adecuada perfusión de medios acuosos. A pesar de que el alginato es un polímero aprobado para aplicaciones biomédicas, su procesamiento para obtener membranas a través del electrohilado enfrenta considerables obstáculos. El objetivo de este trabajo es obtener un método eficiente para producir nanofibras entrecruzadas de alginato (NaAlg) y alcohol polivinílico (PVA) utilizando un baño de The use of nanotechnology in tissue engineering is of great importance for regenerating skin injuries (Asadian et al., 2022). In this regard, nanofiber scaffolds have emerged as a powerful tool, providing structural and functional advantages that closely mimic the native extracellular matrix (ECM) (Arida et al., 2021; Wu et al., 2024). By supporting cellular adhesion and proliferation, nanofiber scaffolds not only act as physical barriers but also actively participate in biochemical signaling pathways crucial for tissue repair (Bolívar et al., 2021). The superior performance of nanofiber scaffolds stems from their biomimetic properties, including a high surface area-to-volume ratio and enhanced surface energy, which promote interactions with biological environments (Wang et al., 2013). Numerous studies have demonstrated that nanofiber-based dressings accelerate healing processes,

reduce scar formation, and support the proliferation of criti-

cal cell types, such as fibroblasts and keratinocytes, in vitro

and in vivo conditions (Meng et al., 2024).

coagulación con CaCl, en el proceso de electrohilado con agujas simple (SN) y coaxial (CN). Se estudiaron los efectos

de la relación molar para SN, el voltaje y la distancia para CN,

identificando condiciones óptimas a 70 % NaAlg for SN, y

15 cm entre la aguja y el colector para CN, ambos sistemas

a 0.1 ml/h y 19 kV. Las nanofibras entrecruzadas resultaron

en diámetros de 70  $\pm$  17 y 124  $\pm$  20 nm para las SN y CN ex-

hibiendo una morfología bien definida e interconectividad.

Se confirmó por FTIR la interacción por carboxilacion con

calcio, entre NaAlg y CaCl<sub>2</sub>. Estudios in vitro de CN NaAlg-PVA

utilizando células de fibroblastos JB6 demostraron una tasa

de proliferación celular del 124 %, lo que indica un potencial

significativo para la aplicación de estas nanofibras en la cica-

Palabras clave: Ingeniería de tejidos; heridas de piel; nanofi-

bras de PVA/alginato; electrohilado coaxial.

trización de heridas.

INTRODUCTION

\*Author for correspondence: Rafael Ramírez Bon, Tonantzi Pérez Moreno e-mail: rrbon@cinvestav.mx; tonantzi.perez@uaq.mx

Received: April 15, 2025 Accepted: September 10, 2025 Published: October 29, 2025

There are many techniques to produce nanofibers; some are self-assembly, template synthesis, freeze-drying, electrospinning, and others (Wang et al., 2019; Ghosh et al., 2021). Particularly, electrospinning, a widely adopted method for nanofiber production, offers versatility in fabricating materials from both natural and synthetic polymers (Xue et al., 2019; Wang et al., 2020). This technique employs an electric field to draw polymer solutions into continuous fibers with diameters in the nanometer range. The adaptability of electrospinning lies in its ability to process a diverse array of biopolymers, including polyvinyl alcohol (PVA) (Islam and Karim, 2010), polyethylene oxide (PEO) (Safi et al., 2007; Nista et al., 2015), gelatin (Majidi et al., 2018), alginate (Alg) (Sadeghi-Aghbash et al., 2022), among others. Sodium alginate, a natural polymer derived from brown algae, has gained attention in biomedical applications due to its excellent biocompatibility, biodegradability, and mild gelation properties mediated by divalent cations such as calcium ions (Ching et al., 2017; Rathee et al., 2024). However, the electrospinning of pure alginate poses significant challenges due to its high viscosity, limited molecular flexibility, and inability to form stable electrospun jet (Taemeh et al., 2020). To overcome these limitations, alginate is often blended with complementary polymers like PVA, which is widely used in biomedical applications because of its water solubility, nontoxic nature, and compatibility with biological systems (Tang et al., 2019; Jadbabaei et al., 2021). This polymer enhances the electrospinnability of alginate by reducing solution viscosity and enabling the formation of continuous fibers. The resulting NaAlg/PVA blends exhibit improved mechanical stability, processability, and biological properties, making them promising candidates for wound healing applications (Coşkun et al., 2010; Aloma et al., 2020; Fahma et al., 2022).

The electrospinning process can be optimized by using accessory steps, such as a drum rotation at high speed, which modifies the collector and promotes the formation of aligned fibers (Li et al., 2021). Modifications to the electrospinning process, such as using coaxial needles (CN) and integrating coagulation baths, have demonstrated effectiveness in overcoming key challenges (Qin, 2017; Haider et al., 2018; Mohammadalizadeh et al., 2022). Coagulation baths serve a dual purpose: they stabilize fibers by crosslinking alginate chains with calcium ions (Ca2+). This arrangement facilitated immediate ionic crosslinking of alginate upon contact with the CaCl<sub>3</sub> solution, stabilizing the fibers and enhancing their mechanical properties (Nie et al., 2008; Barber et al., 2013). The integration of the coagulation bath allowed simultaneous crosslinking and collection, improving the overall efficiency and functionality of the electrospinning process (Barber et al., 2013). Additionally, CaCl, enables rapid gelation upon contact. Compared to other agents, CaCl, is cost-effective, widely available, and poses a low risk of over-crosslinking, which can compromise material flexibility (Li et al., 2016; Abedini et al., 2023).

In this work, a novel bath/electrospinning method to achieve NaAlg and PVA crosslinked nanofibers using two

needle systems was performed. Systematically the impact of processing parameters on fiber morphology in the absence of the crosslinked solution were exanimated, followed by an assessment of the crosslinking efficiency with the coagulation bath and then biological performance. The first system is a conventional electrospinning process with a SN where nanofibers were electrospun from a precursor solution composed of a blend of NaAlg and PVA polymers at two different molar ratios, exhibiting a well-defined morphology at higher concentrations of NaAlg compared to reported works. The second system is an electrospinning process that employs a CN, where the inner and outer capillaries conduct the PVA and NaAlg solutions, respectively. This resulted in the fabrication of a novel core-shell structure of pure NaAlg as the shell. The third method, following the optimization of crosslinked fibers that were not readily soluble upon contact with water, consists in collecting the fibers in a coagulation bath with Ca<sup>2+</sup> to crosslink the polymers during the fibers production, both SN and CN systems were used, where NaAlg is permitted to interact with the ions to produce membranes with well-defined size and interconnected morphology, devoid of cytotoxic components allowing qualitative water resistance. Finally, the in vitro cytotoxicity of the obtained CN NaAlg-PVA membrane was assessed to evaluate their biocompatibility, and cell viability around 124 % at 48 h indicated a significant potential use as scaffolds in tissue regeneration.

# MATERIAL AND METHODS

#### **Materials**

Polyvinyl alcohol (PVA, MFCD00081922, Mw 89,000 – 98,000, containing vinyl acetate impurities), sodium alginate (NaAlg, MFCD00081310), and calcium chloride (CaCl<sub>2</sub>) were obtained from Sigma-Aldrich.

#### Electrospinning of blended sodium alginate and PVA

NaAlg was dissolved at a concentration of 2 % (w/v) in distilled water under continuous magnetic stirring at room temperature. PVA was dissolved at 10 % (w/v) in distilled water, with magnetic stirring maintained at  $80 \pm 5$  °C for 2 h to ensure complete solubilization. For the single-needle electrospinning process, as shown in Fig. 1, polymer mixtures were prepared with NaAlg and PVA at ratios of 30:70 and 70:30, respectively, the names of the samples are listed in Table 1.

**Table 1.** Samples nomenclature according to the different methods of electrospinning used.

**Tabla 1.** Nomenclatura de las muestras de acuerdo a los distintos métodos de electrohilado utilizados.

Sample	Method
NaAlg:PVA (30:70)	Simple
NaAlg:PVA (70:30)	Simple
NaAlg-PVA	Coaxial
CN CaAlg-PVA	Coaxial and Bath coagulation
CaAlg:PVA	Simple and Bath coagulation

The electrospinning of NaAlg and PVA blend fibers was carried out using a syringe mounted on a KD Scientific model 200 injector pump. A Bertan 230 series voltage source supplied the required electric field, and the fibers were collected on an aluminum plate. A 20 G needle was used for the polymer mixture, which was electrospun at a controlled flow rate of 0.1 mL/h. The distance between the needle tip and the collector was optimized at 10 cm, while the applied voltage was 19 kV.

#### **Electrospinning of coaxial alginate and PVA fibers**

In the coaxial needle system, as shown in Fig. 1, the inner capillary was loaded with the PVA solution, while the outer capillary contained the alginate solution supplemented with Triton-X-100 at 0.05 % (w/v) to decrease the surface tension (Taemeh et al., 2020). In the electrospinning setup an 18 G needle was used for the outer capillary containing the alginate solution (Singaravelu et al., 2024), while a 26 G needle was employed for the inner capillary loaded with the PVA solution (Silva et al., 2019). Electrospinning was performed under similar conditions as the single-needle system, with a flow rate of 0.1 mL/h, a tip-to-collector distance of 15 to 20 cm, and an applied voltage of 19 kV.

## **Crosslinked arrangement**

For crosslinking, the electrospinning setup incorporated a vertical orientation of the syringe and collection plate. The collection plate was submerged in a Petri dish containing a coagulation bath composed of 0.5 % (w/v) CaCl<sub>3</sub> in distilled water with ethanol at a 5:1 ratio (Li et al., 2016).

#### **Physicochemical Characterization**

Fourier Transform Infrared (FT-IR) spectroscopy was conducted using a Perkin Elmer GX Spectrum One model (United States) spectrophotometer in the range of 4000 - 650 cm<sup>-1</sup>

in ATR mode. This analysis enabled the identification of functional groups and molecular interactions present in the polymer blends and crosslinked fibers. Surface morphology and cross-section were examined using a JEOL JSM-7610F (Japan) field emission scanning electron microscope (SEM) operated at an accelerating voltage of 5 kV. Prior to imaging, samples were coated with a thin layer of gold foil to enhance conductivity and improve resolution, allowing for detailed visualization of fiber structure and uniformity.

#### Biological experiments on the membranes

JB6 fibroblast cells from mouse skin were proliferated in T25 flasks with a surface treatment to ensure optimal cell attachment and growth in DMEM (5 % FBS and 1 % antibiotic) and were maintained at 37 °C in a humidified incubator with 5 % CO<sub>2</sub>. The membranes were neutralized by immersion in DMEM medium until a red coloration indicated pH stabilization. Following neutralization, the membranes were transferred to a 24-well plate for evaluation of cell viability using the 3 - (4,5 - dimethylthiazol - 2 - yl) -2,5 - diphenyltetrazolium bromide (MTT) assay.

JB6 fibroblast cells were seeded in sterile 96-well flatbottom microplates at a 2 1.5 x 10<sup>4</sup>/well onto the membranes, cultured in supplemented DMEM media, and incubated for 24 and 48 h. As positive control cells were seeded under normal culture conditions and considered as 100 % in the equation. The films used as controls were obtained with the same solutions of NaAlg:PVA (70:30) and NaAlg by coating at room temperature. After the incubation period, the media were removed, and 100 µL of fresh media were added into each well with 10 µL of MTT solution (0.5 mg/mL) following another incubation for four hours. The formazan crystals formed by metabolically active cells were dissolved with 10 µL of DMSO, and transferred to a 96 well plate and their absorbance was measured at 595 nm using an IMark ELISA

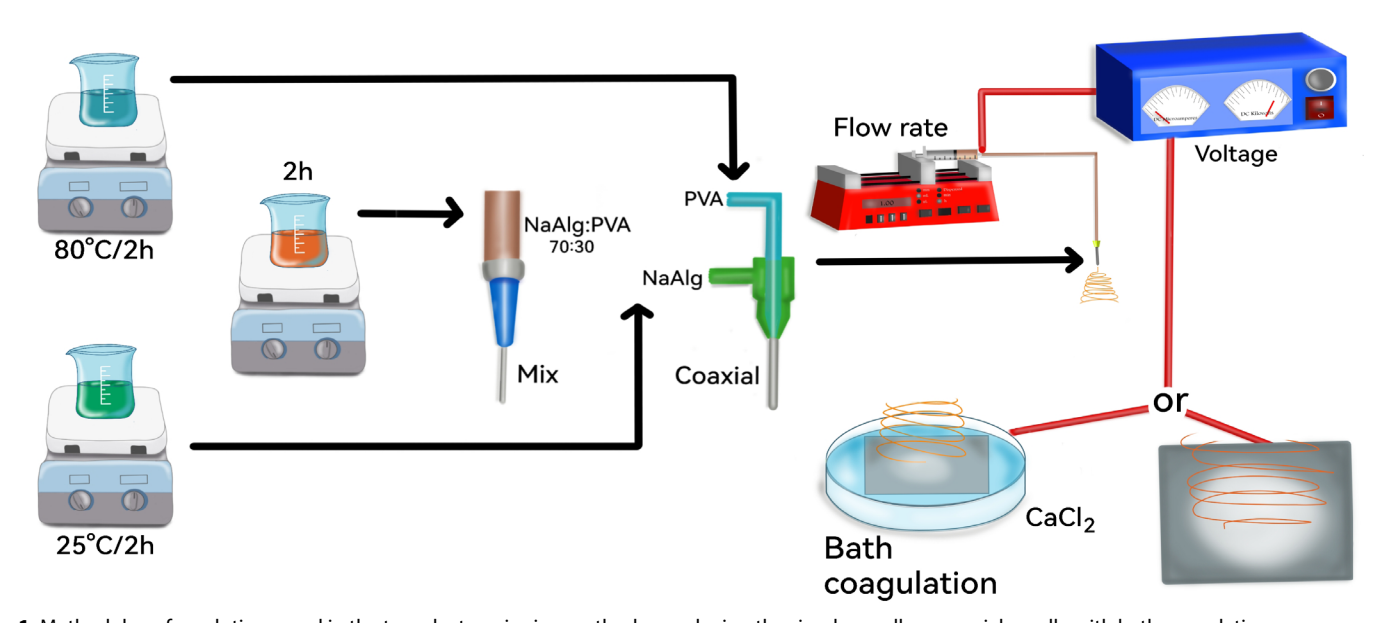


Fig. 1. Methodology for solutions used in the two electrospinning methods, employing the simple needle or coaxial needle with bath coagulation. Fig, 1. Metodología para las soluciones usadas en los dos métodos de electrohilado, empleando la aguja simple o coaxial con el baño de coagulación.

Eq. (1)

microplate reader (California, United States). The cell viability (%), compared with control wells containing cells without treatment, was calculated using the following Equation (1) (Riss *et al.*, 2016):

Cell viability (%) = [Abs(X) test/Abs(Y) control] \* 100 %,

## **RESULTS AND DISCUSSION**

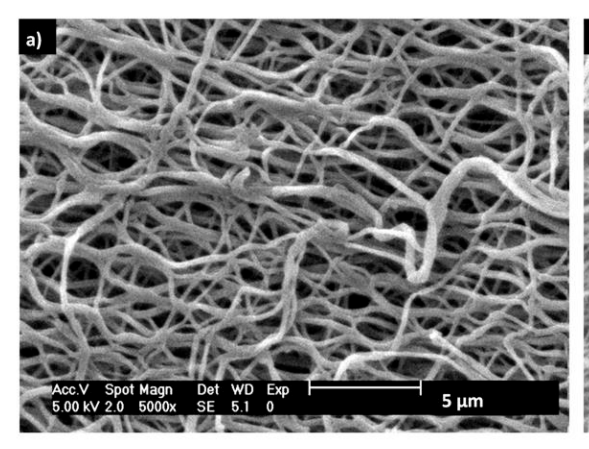
Two samples varying NaAlg:PVA molar ratios (30:70 and 70:30) were analyzed using SEM (Fig. 2). The analysis of these SEM images was performed using Image J software to determine the fiber diameter; in both cases, the analyzed sample consisted of 100 fibers. The SEM micrograph in Fig. 2a corresponds to fibers produced of NaAlg:PVA (30:70). The morphology of these fibers exhibited branching and a slight degree of crisscrossing, while maintaining a generally welldefined structure. The measured average fiber diameter was 127  $\pm$  8 nm, with a PD index of 0.06. In contrast, the fibers produced of NaAlg:PVA (70:30), shown in Fig. 2b, displayed notably different morphological characteristics. These fibers were thinner on average, with a measured diameter of 114 ± 33 nm, with a PD index of 0.28. Unlike the NaAlg:PVA (30:70) fiber system, no branching was observed, and the fiber density was significantly higher. This increased density contributed to a more uniform distribution of fibers as previously reported (Kinler et al., 2022). Both membranes were carried on at 19 kV, a tip-to-collector distance of 10 cm, and a flow rate of 0.1 mL/h. Additionally, after the electrospinning process was completed, these membranes dissolved upon contact with water.

The influence of the collector-to-needle distance on the morphology of CN NaAlg-PVA fibers was investigated, as illustrated in Fig. 3. This arrangement was specifically designed to overcome the challenges associated with the electrospinnability of alginate by leveraging the conformational charge alignment of its polymer chains. In Fig. 3a, the fibers were produced at a collector-to-needle distance of

10 cm. At this short distance, incomplete solvent evaporation led to the presence of both droplets and fibers in the sample (Suresh et al., 2020). The resultant fibers exhibited a bead-on-string morphology, and their average diameter was measured at  $134 \pm 18$  nm, with a PD index of 0.13. These observations indicate that the distance was insufficient to allow for stable jet elongation and proper fiber formation. Increasing the distance to 15 cm resulted in improved fiber morphology, as shown in Fig. 3b. The fibers had an average diameter of 124 ± 20 nm, with a PD index of 0.16. While droplet formation persisted, it occurred less frequently and was distributed randomly across the sample. At a distance of 18 cm (Fig. 3c), the fiber diameter decreased to  $104 \pm 57$  nm, with a PD index of 0.54. The morphology of the fibers was less uniform, but with no visible droplets. However, some fibers exhibited branching and were poorly interconnected, likely due to increased stretching of the polymer jet at this optimized distance. These defects could decrease membrane porosity and influence the membrane resistivity (Mata et al., 2022; Türkoğlu et al., 2024).

These results indicate that 15 cm provides a balance between solvent evaporation and jet stability, leading to the most favorable fiber formation conditions. These parameters ensured a stable coaxial jet and enabled the fabrication of nanofibers with well-defined morphology and enhanced structural integrity.

Finally, the fiber quality deteriorated significantly when the distance was increased to 20 cm (Fig. 3d). The samples exhibited film-like structures rather than distinct fibers. This transition from fiber to film was attributed to excessive diffusion of the polymer jets, which facilitated fusion between fibers during collection. This phenomenon is influenced by variations in electric field affecting jet stability (Joy et al., 2021) or tip-to-collector distance (Türkoğlu et al., 2024). Additionally, the presence of droplets and watermarks further confirmed material agglomeration and incomplete jet stabilization under these conditions. Furthermore, the core-shell configuration of the fibers shown in Fig. 3b was



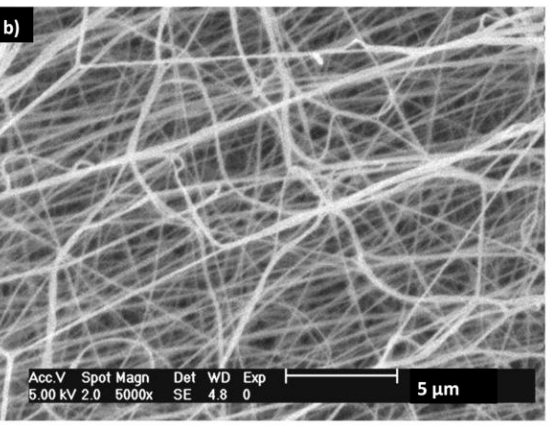


Fig. 2. SEM micrographs of NaAlg and PVA mixed nanofibers electrospun at 19 kV, a tip-to-collector distance of 10 cm, and a flow rate of 0.1 mL/h: (a) fibers synthesized with NaAlg:PVA (30:70), and (b) fibers synthesized with NaAlg:PVA (70:30).

Fig. 2. Micrografias de SEM de las nanofibras de la mezclas de NaAlg y PVA a 19 kV, una distancia entre el colector y la aguja de 10 cm, un flujo de 0.1 ml/h: a) fibras sintetizadas NaAlg:PVA (30:70), y b) fibras sintetizadas con NaAlg:PVA (70:30).



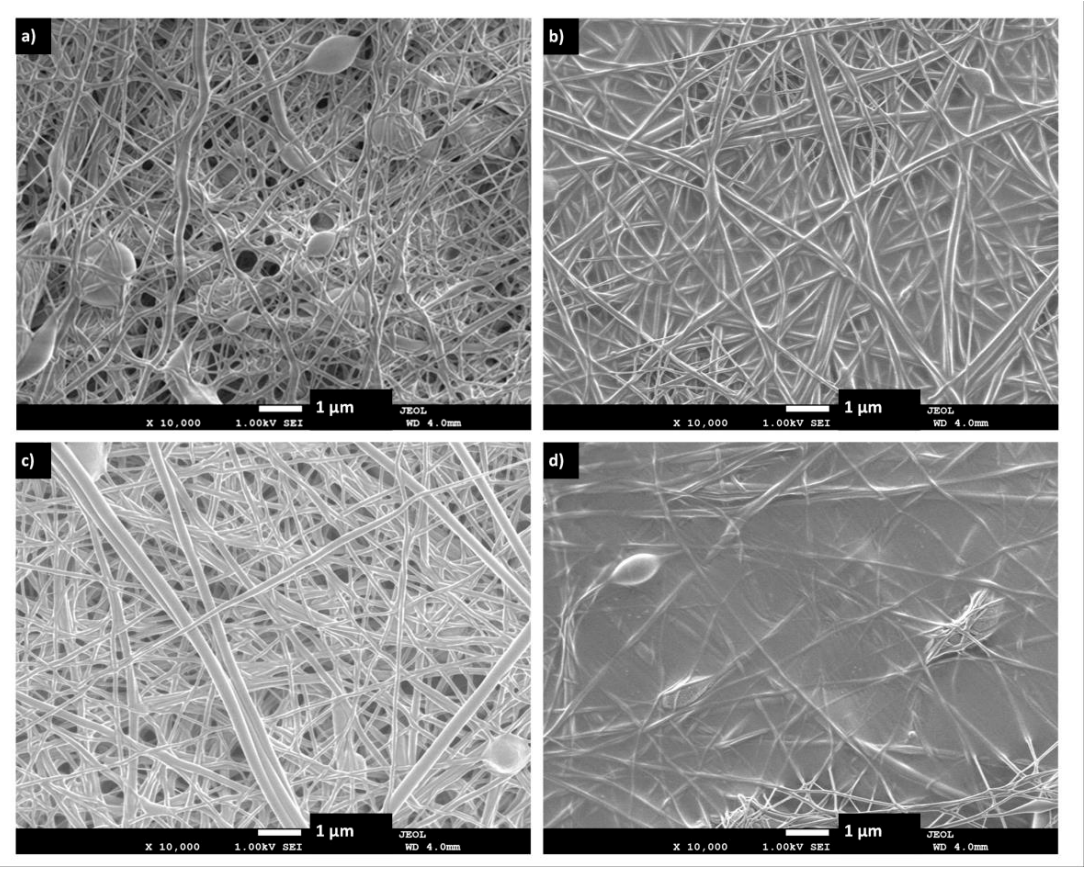


Fig. 3. SEM micrographs of coaxial NaAlg-PVA nanofibers electrospun with PVA as the core and Alg as the shell, under a voltage of 19 kV and a flow rate of 0.1 mL/h, at varying tip-to-collector distances: (a) 10 cm, (b) 15, (c) 18 cm, and (d) 20 cm.

Fig. 3. Micrografías de SEM de nanofibras coaxiales electrohiladas de NaAlg-PVA con núcleo de PVA y coraza de Alg, con un voltaje de 19 kV y un flujo de 0.1 ml/h, con una variación de la distancia entre al colector de: 10 cm (a), 15 cm (b), 18 cm (c) y 20 cm (d).

corroborated by their cross-sectional SEM image shown in Fig. 4. This image depicts a solid and dense core structure, and a thin outer (shell) layer with a slightly lower density. The internal phase is attributed to PVA, while the external coating corresponds to NaAlg, highlighting the formation of a core-shell architecture. However, after the electrospinning process was completed, these membranes nearly dissolved upon contact with water.

Therefore, to produce membranes that do not degrade quickly when in contact with an aqueous environment, after determining the conditions to achieve well-defined fibers with both electrospinning methods, the impact of incorporating a coagulation bath containing a CaCl solution as a crosslinking agent was evaluated, with the results shown in Fig. 5. The addition of this bath aimed to enhance fiber stabilization by facilitating ionic crosslinking between alginate chains during collection. Fig. 5a illustrates crosslinked CaAlg:PVA fibers produced using a conventional SN electrospinning system, with the 70:30 mix of NaAlg and PVA at 19 kV, 15 cm and 0.1 mL/h. The fibers had an average diameter of 70  $\pm$  17 nm, with a PD index of 0.24. However, clusters were observed on the surface, indicating incomplete contact between the fibers and the CaCl, solution. This lack of interaction resulted in regions of uncrosslinked material and inconsistent morphology. Moreover, areas of fiber coalescence were identified (Kenawy et al., 2023), attributed to excessive contact between fibers during collection (Fahmy et

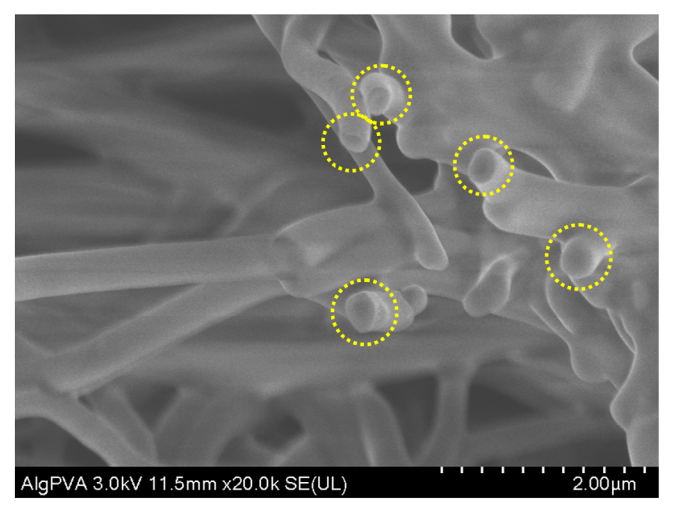
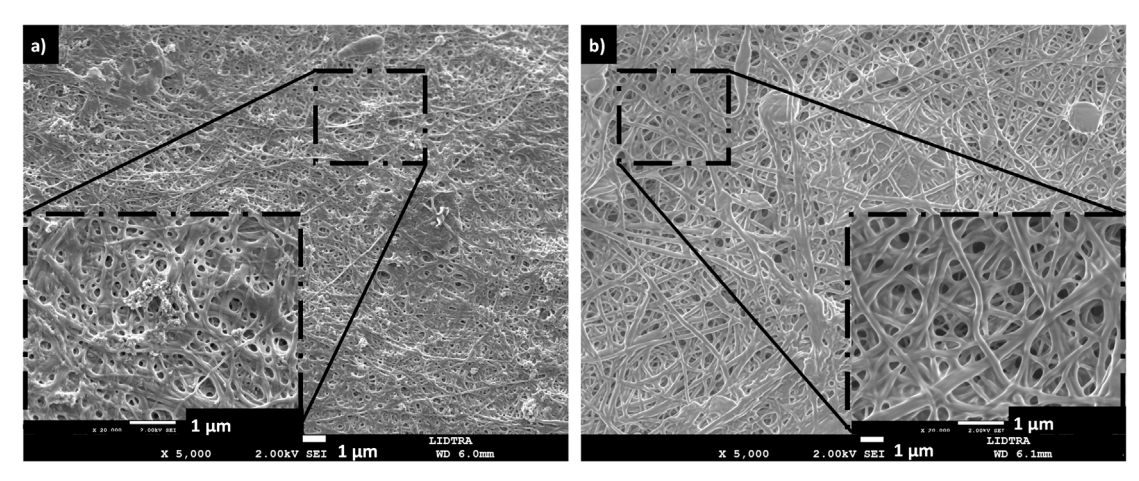


Fig. 4. SEM micrographs of coaxial nanofibers prepared from Alg and PVA, NaAlg-PVA, at 19 kV, 15 cm, 0.1 mL/h.

Fig. 4. Micrografías de SEM de nanofibras coaxiales sintetizadas de Alg y PVA, NaAlg-PVA, a 19 kV, 15 cm, y 0.1 mL/h.



**Fig. 5.** SEM micrographs of nanofibers prepared from Alg and PVA with bath coagulation using CaCl<sub>2</sub> as crosslinker with a) simple system 70:30 CaAlg:PVA at 19 kV, 15 cm, 0.1 mL/h and b) coaxial system CaAlg-PVA at 19 kV, 15 cm and 0.1 mL/h. **Fig. 5.** Micrografías de SEM de nanofibras de Alg y PVA sintetizadas con el baño de coagulación utilizando CaCl<sub>2</sub> como agente de entrecruzamiento con a) el sistema simple de mezcla 70:30 CaAlg:PVA a 19 kV, 15 cm y 0.1 mL/h, y b) sistema coaxial CaAlg-PVA a 19 kV, 15 cm y 0.1 mL/h.

al., 2025). This phenomenon led to a film-like structure, like the material observed for CN NaAlq-PVA fibers in Fig. 3d.

When a coaxial needle system was utilized in conjunction with the coagulation bath, at 19 kV, 15 cm and 0.1 mL/h, significant improvements in fiber morphology were observed, as shown in Fig. 5b. The crosslinked CN CaAlg-PVA fibers had an average diameter of 179 ± 62 nm, with a PD index of 0.34. The fibers formed a cohesive membrane with some interconnected structures, giving the appearance of a braided configuration (Kahya and Gürarslan, 2025). This interconnected morphology can be attributed to the improved stability provided by the coaxial setup. Specifically, the rigid molecular structure of NaAlg and their lack of molecular interweaving often cause droplet accumulation at the needle tip, disrupting the electrospinning process (Wang and Nakane, 2020). These results demonstrate that the use of a coagulation bath effectively enhances the recovery of nanofibers and mitigates droplet formation on the material surface. The addition of CaCl<sub>2</sub> not only supports crosslinking but also improves the joints between fibers, resulting in a more robust and uniform fibrous membrane (Majidi et al., 2018; Miranda et al., 2022).

The interactions between polymers in the synthesized fibers were analyzed using FT-IR spectroscopy. Fig. 6 shows the spectra of the starting materials, NaAlg and PVA, as well as the mixed NaAlg:PVA (70:30) and NaAlg:PVA (30:70) fibers produced at varying molar ratios. The pristine PVA spectrum exhibits characteristic vibrational signals, including a broad band at 3347 cm<sup>-1</sup> corresponding to OH stretching (Aloma *et al.*, 2020) and bands at 2946 cm<sup>-1</sup> and 2906 cm<sup>-1</sup> associated with CH<sub>2</sub> stretching (Hulupi and Haryadi, 2019). Additional signals include a band at 1735 cm<sup>-1</sup>, indicating a C=O double bond, and a band at 1610 cm<sup>-1</sup>, attributed to the asymmetric stretching of carboxylate salts (Giz *et al.*, 2020). Symmetric stretching is observed at 1582 cm<sup>-1</sup>, CH-OH vibrations at 1455 cm<sup>-1</sup>, and CH-OH bending vibrations at 1325 cm<sup>-1</sup> (Islam and Karim, 2010). Bands at 945 cm<sup>-1</sup>, 886 cm<sup>-1</sup>,

and 829 cm<sup>-1</sup> correspond to CH<sub>2</sub> rocking vibrations, B-C1-H deformations, and C-C stretching, respectively (Jadbabaei *et al.*, 2021). The NaAlg spectrum includes characteristic bands such as the C=O double bond at 1752 cm<sup>-1</sup> (Mohammadi *et al.*, 2019), CH-OH vibrations at 1453 cm<sup>-1</sup>, and C-O stretching of the pyranosyl ring at 1183 cm<sup>-1</sup> (Chen *et al.*, 2021). Bands at 956 cm<sup>-1</sup> and 868 cm<sup>-1</sup> correspond to C-O stretching with contributions from C-C-H and COH deformation, and B-C1-H interactions, respectively (Daemi and Barikani, 2012).

The FT-IR spectrum of fibers synthesized with a NaAlg:PVA (30:70) is shown in Fig. 6. The spectrum displays characteristic signals from the PVA component, with notable shifts observed in the COOH stretching region. Specifically, bands originally present in the PVA spectrum at 1455 cm<sup>-1</sup> and 1325 cm<sup>-1</sup> shifted to the right at 1422 cm<sup>-1</sup> and to left at 1347 cm<sup>-1</sup>, respectively (the vertical dashed lines indicate

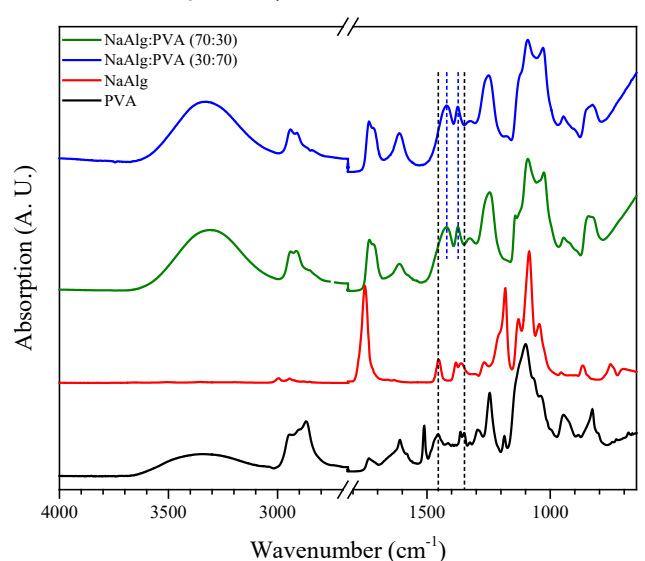


**Fig. 6.** Infrared spectra of NaAlg, PVA, and the membranes obtained using SN systems with 30:70 and 70:30 polymer ratios.

**Fig. 6.** Espectro infrarrojo de NaAlg, PVA y las membranas obtenidas utilizando el sistema de SN con las relaciones molares de 30:70 y 70:30.



Volume XXVII

these shifts). These shifts suggest compression of the polymer main chain, resulting in restricted molecular motion (Shalumon et al., 2011). Similar spectral shifts were observed in fibers synthesized with NaAlq:PVA (30:70), further confirming the influence of NaAlg and PVA interactions on the fiber structure. These interactions between COOH and OH groups indicate a high density of intermolecular interactions within the polymer chains (Arthanari et al., 2016). The findings are consistent with SEM observations in Fig. 2a, where restricted fiber mobility was evident, further validating the spectral data.

For the coaxial fibers (Fig. 7), the FT-IR spectrum shows significant surface interactions dominated by PVA and NaAlq signals. Shifts in PVA bands were observed, moving from  $3339 \, \text{cm}^{-1}$ ,  $1454 \, \text{cm}^{-1}$ , and  $1382 \, \text{cm}^{-1}$  to  $3316 \, \text{cm}^{-1}$ ,  $1429 \, \text{cm}^{-1}$ , and 1373 cm<sup>-1</sup>, respectively. These shifts indicate substantial surface-level interactions between the polymers (Arthanari et al., 2016). However, the reinforcement phase corresponds to NaAlg, which has no signal at 1611 cm<sup>-1</sup>, meaning that the polymer chains of the components have not been crosslinked. This result aligns with the SEM observations in Fig. 3, where weak interconnectivity and lack of crosslinking were evident.

Finally, when the coagulation bath was introduced to the system, the resulting fibers exhibited strong interconnectivity, indicating successful crosslinking. As shown in Fig. 8, the FT-IR spectrum of these fibers includes the band at 1612 cm<sup>-1</sup>, confirming carboxylate salt formation and crosslinking (Giz et al., 2020). The presence of CaCl<sub>2</sub> in the coagulation bath facilitated the formation of a reticular network within the fibers, enhancing their structural stability (Azmia et al., 2024). Unlike in the coaxial system without the coagulation

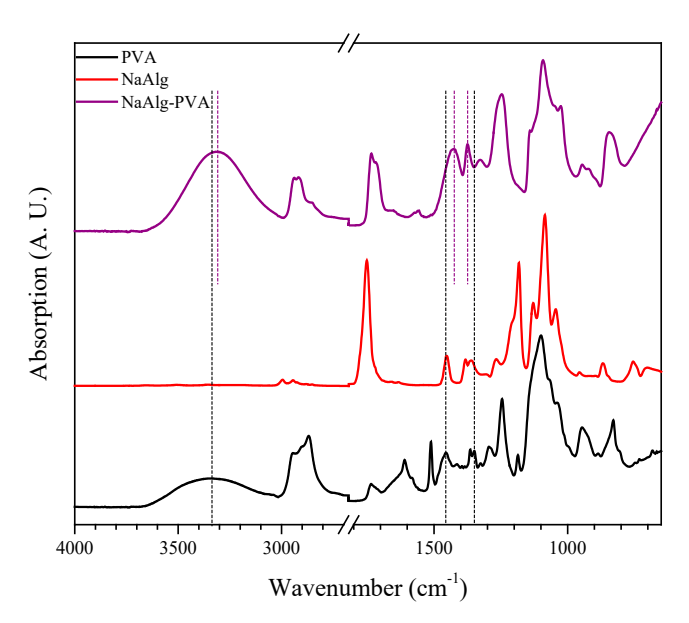


Fig. 7. Infrared spectra of NaAlq, PVA and the nanofibers produced by the CN electrospinning system, with PVA as the core and NaAlg as the shell (NaAlg-

Fig. 7. Espectro infrarrojo de NaAlg, PVA y las nanofibras derivadas del sistema de electrohilado coaxial, con PVA como el núcleo y NaAlg como la coraza (NaAlg-PVA).

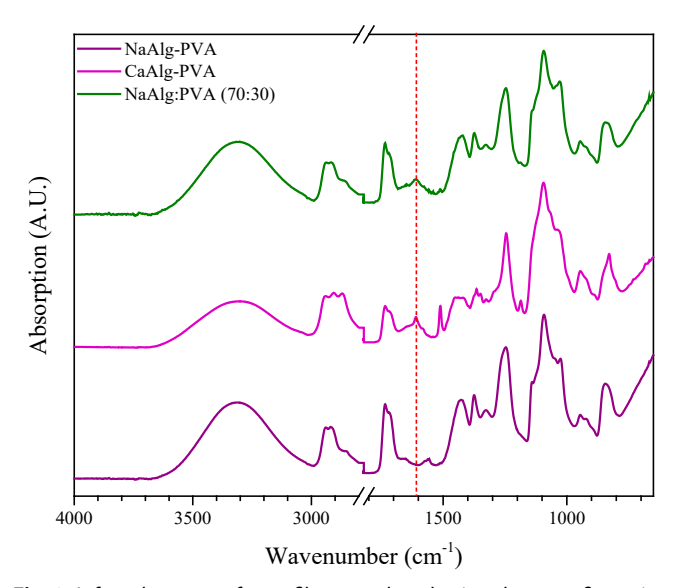
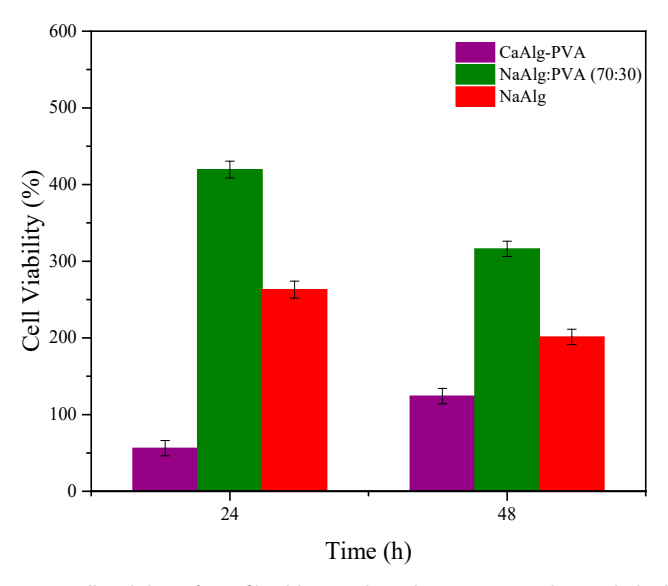


Fig. 8. Infrared spectra of nanofibers produced using three configurations: (a) a SN system with a NaAlg:PVA (70:30), (b) a CN system NaAlg-PVA, and (c) a CN crosslinked system CaAlg-PVA, incorporating a CaCl, coagulation bath. Fig. 8. Espectro infrarrojo de nanofibras producidas por las tres configuraciones: (a) sistema SN de la mezcla de NaAlg:PVA (70:30), (b) el sistema CN NaAlg-PVA, y (c) sistema CN y entrecruzamiento CaAlg-PVA con CaCl, en el baño de coagulación.

bath, no additional peak shifts were observed, suggesting that the crosslinking process relied on ionic interactions rather than new chemical bond formation. These findings complement the SEM results shown in Fig. 5, which highlight the enhanced fiber morphology and interconnectivity achieved with the coagulation bath.

The cross-linked coaxial membrane was studied with JB6 fibroblasts from mouse skin to determine cell viability. During the experiment, the crosslinked CN CaAlg-PVA fibers decreased in size due to interaction through hydrogen bonds with the red phenol present in the culture medium (Sreedhar et al., 2016), which could dissolve the clumps on the membrane and modify the morphology of the fibers on the plate. At 24 h, the cell viability on the crosslinked membranes reached 52 %, as shown in Fig. 9. This viability level could be attributed to the potential ability of fibroblasts to stabilize and adhere to the surface of the fibers, which may provide sufficient anchorage points to support initial cell attachment and promote cellular interactions. However, control samples exhibited higher cell viability during the same period. This disparity can be attributed to the larger continuous surface area of the films, which at the beginning may have facilitated greater cell adhesion compared to the porous structure of the fiber membranes (Khalili and Ahmad, 2015). This trend aligns with previous studies indicating that planar surfaces often outperform fibrous scaffolds in supporting initial cell adhesion (Bružauskaitė et al., 2015). After 48 h, the cell viability on the crosslinked CN CaAlg-PVA membranes increased significantly to 124 %, suggesting that the fibroblasts may not only have survived but also potentially proliferated effectively on the fibers. This period is important because it is a reference of when the contact between the skin and



**Fig. 9.** Cell viability of JB6 fibroblasts cultured in contact with crosslinked CaAlg-PVA nanofibers, NaAlg:PVA (70:30) films, and pure NaAlg films. The viability was assessed at 24 and 48 h using an MTT assay. All values represent the average values of three experiments performed in duplicate.

**Fig. 9.** Viabilidad celular de fibroblastos JB6 cultivadas en contacto con las nanofibras entrecruzadas CaAlg-PVA, películas de NaAlg:PVA (70:30), y películas de NaAlg puro. La viabilidad se realizó a 24 y 48 h usando el ensayo MTT. Todos los valores representan el promedio de tres experimentos realizados por duplicado.

the biomaterial is achieved in the first 12 h of the process of primary matrix formation and wound healing to 48-72 h of the inflammatory stage (Ansari and Darvishi, 2024).

In contrast, cell viability on the control films decreased to approximately 100 %, suggesting that the random distribution and porosity of the fiber membranes provided superior conditions for sustained cell proliferation. When compared to previous studies, where fibers made from similar biopolymers achieved 40 % cell viability after 8 days, the crosslinked CN CaAlg-PVA membranes demonstrated markedly superior performance (Fahma et al., 2022). During the evaluation of PVA nanofibers produced by electrospinning, no cytotoxic effects were observed when the MTT test was carried out and in general, the scaffolds generated with PVA demonstrated good biocompatibility which was improved by the addition of collagen (Khalaji et al., 2021). Similar effect could be observed when cellulose nanofibrils (T-CNFs) embedded in Alg and PVA solution were evaluated to obtain mineralized hydrogels, where the results shown reveal that these materials promote cell proliferation (Abouzeid et al., 2022). It has been found that nanofibers with concentrations of up to 2.5 % of PVA have shown that they are a good option as biological dressing scaffolds since PVA nanofibers manage to stimulate cell proliferation and promoted cell viability, although it was found that when the nanofibers incorporate growth factors, cell proliferation and adhesion increase, in no case cytotoxic effects were identified (Asiri et al., 2021). The significant increase in cell viability at 48 h highlights the potential of these membranes to support early-stage tissue.

# **CONCLUSIONS**

Using a bath coagulation/electrospinning method enables the production of crosslinked nanofibers based on PVA and NaAlg with well-defined size and morphology. First, the optimization require the evaluation of the simple and coaxial needle electrospinning systems without the bath coagulation; in the case of the simple system configuration with PVA and NaAlg, the results suggested that the obtained SN NaAlg:PVA fibers exhibit blend characteristics evidenced by features in the IR spectra revealing a physical interaction between the components, where the PVA allows the electrospinning process of NaAlg to form the resulting fibers. And for the CN, the resulting fibers have the core-shell structure as shown by cross-section SEM images, and the IR spectrum reveals that the components converge with only physical interaction. These CN NaAlg-PVA facilitated the fabrication of a novel core-shell structure with pure NaAlg as the shell, which has only reported as mixture with other polymers.

With the conditions optimized, the coagulation bath enabled the cross-linking of alginate fibers through the formation of carboxylate-calcium bridges when interacting with calcium ions. This produced fiber membranes with a well-defined interconnected fibrous morphology and a uniform size distribution. Additionally, a non-solvent upper contact with water allowed their cytotoxic evaluation, where the cell viability of the novel membrane CN CaAlg-PVA showed an increase of 124 % in cell viability after 2 days; period which is important since the contact between the skin and the biomaterial in wound healing occurs around this time. In comparison to other similar biomaterials, which showed 40 % cell viability after 7 days, our system demonstrated significantly higher cell viability, reaching 31 % more than the highest value reported. Notably, the proposed fibers system is simpler than those previously reported. These results suggest that the composite biomaterial developed in this study has potential for use in tissue regeneration, but further studies are recommended.

#### **ACKNOWLEDGMENTS**

The use of LIDTRA facilities is greatly acknowledged. Also, MSc Eleazar Gómez, MSc Manuel Aguilar Franco, and MSc Araceli Mauricio are acknowledged for their helpful assistance with the SEM and IR analysis.

#### **CONFLICTS OF INTEREST**

The authors declare not conflicts of interest.

#### REFERENCES

Abedini, A.A., Pircheraghi, G. and Kaviani, A. 2023. The role of calcium crosslinking and glycerol plasticizing on the physical and mechanical properties of superabsorbent: Alginate/Quince Seed Gum films. Journal of Polymer Research. 30(1), 1-14.

Abouzeid, R.E., Salama, A., El-Fakharany, E.M. and Guarino, V. 2022. Mineralized polyvinyl alcohol/sodium alginate hydrogels incorporating cellulose nanofibrils for bone and wound healing. Molecules. 27(3), 697.



- Aloma, K.K., Sukaryo, S., Fahlawati, N.I., Dahlan, K. and Oemar, S. 2020. Synthesis of nanofibers from alginate-polyvinyl alcohol using electrospinning methods. Macromolecular Symposia. 391(1), 1900199.
- Ansari, M. and Darvishi, A. 2024. A review of the current state of natural biomaterials in wound healing applications. Frontiers in Bioengineering and Biotechnology, 12, 1309541.
- Arida, I.A., Ali, I.H., Nasr, M. and El-Sherbiny, I.M. 2021. Electrospun polymer-based nanofiber scaffolds for skin regeneration. Journal of Drug Delivery Science and Technology. 64, 102623.
- Arthanari, S., Mani, G., Jang, J.H., Choi, J.O., Cho, Y.H., Lee, J.H., Cha, S.E., Oh, H.S., Kwon, D.H. and Jang, H.T. 2016. Preparation and characterization of gatifloxacin-loaded alginate/ poly (vinyl alcohol) electrospun nanofibers. Artificial cells, nanomedicine, and biotechnology. 44(3), 847-852.
- Asadian, E., Masoudifar, R., Pouyanfar, N. and Ghorbani-Bidkorbeh, F. 2022. Nanotechnology-based therapies for skin wound regeneration. Emerging Nanomaterials and Nano-based Drug Delivery Approaches to Combat Antimicrobial Resistance, 485-530.
- Asiri, A., Saidin, S., Sani, M.H. and Al-Ashwal, R.H. 2021. Epidermal and fibroblast growth factors incorporated poly-vinyl alcohol electrospun nanofibers as biological dressing scaffold. Scientific Reports. 11(1), 1-14.
- Azmia, R.N., Fadhil, M.T., Deril, S. and Dimas, R.N. 2024. Synthesis and characterization of chitosan/alginate hydrogel using CaCl<sub>2</sub> as a crosslinking agent. Materials Science Forum. 1140, 85-91.
- Barber, P.S, Griggs, C.S., Bonner, J.R. and Rogers, R.D. 2013. Electrospinning of chitin nanofibers directly from an ionic liquid extract of shrimp shells. Green Chemistry. 15(3), 601-
- Bolívar-Monsalve, E.J., Alvarez, M.M., Hosseini, S., Espinosa-Hernandez, M.A., Ceballos-González, C.F., Sanchez-Dominguez, M., Shin, S.R., Cecen, B., Hassan, S., Di Maio, E. and Trujillo-De Santiago, G. 2021. Engineering bioactive synthetic polymers for biomedical applications: a review with emphasis on tissue engineering and controlled release. Materials Advances. 2(14), 4447-4478.
- Bružauskaitė, I., Bironaitė, D., Bagdonas, E. and Bernotienė, E. 2015. Scaffolds and cells for tissue regeneration: different scaffold pore sizes—different cell effects. Cytotechnology, 68(3), 355.
- Chen, J., Yang, Z., Shi, D., Zhou, T., Kaneko, D. and Chen, M. 2021. High strength and toughness of double physically cross-linked hydrogels composed of polyvinyl alcohol and calcium alginate. Journal of Applied Polymer Science, 138(10), 49987.
- Ching, S.H., Bansal, N. and Bhandari, B. 2017. Alginate gel particles-A review of production techniques and physical properties. Critical Reviews in Food Science and Nutrition, 57(6), 1133-1152.
- Coşkun, G., Karaca, E., Ozbek, S. and ÇavuşoĞlu, I. 2010. In vivo evaluation of electrospun poly (vinyl alcohol)/sodium alginate nanofibrous mat as wound dressing. Tekstil ve Konfeksiyon, 20, 290-298.
- Daemi, H. and Barikani, M. 2012. Synthesis and characterization of calcium alginate nanoparticles, sodium homopolymannuronate salt and its calcium nanoparticles. Scientia Iranica, 19(6), 2023-2028.

- Fahma, F., Febiyanti, I., Lisdayana, N., Sari, W., Noviana, D., Yunus, M., Thomryes, G., Kadja, M. and Kusumaatmaja, A. 2022. Production of polyvinyl alcohol-alginate-nanocellulose fibers. Starch - Stärke. 74, 2100032.
- Fahmy, A., Badry, R., Mabied, A.F., Wassel, A.R., Khafagy, R.M. and Ibrahim, M.A. 2025. Application of electrospun polyvinyl alcohol/sodium alginate nanofibers as biosensor. Journal of Inorganic and Organometallic Polymers and Materials, 1-21.
- Ghosh, T., Das, T. and Purwar, R. 2021. Review of electrospun hydrogel nanofiber system: Synthesis, Properties and Applications. Polymer Engineering and Science. 61(7), 1887-1911
- Giz, A.S., Berberoglu, M., Bener, S., Aydelik-Ayazoglu, S., Bayraktar, H., Alaca, B.E. and Catalgil-Giz, H. 2020. A detailed investigation of the effect of calcium crosslinking and glycerol plasticizing on the physical properties of alginate films. International Journal of Biological Macromolecules. 148, 49-55.
- Haider, A., Haider, S. and Kang, I.K. 2018. A comprehensive review summarizing the effect of electrospinning parameters and potential applications of nanofibers in biomedical and biotechnology. Arabian Journal of Chemistry. 11(8), 1165-1188.
- Hulupi, M. and Haryadi, H. 2019. Synthesis and characterization electrospinning PVA nanofiber-crosslinked glutaraldehyde. Materials Today: Proceedings. 13, 199-204.
- Islam, M.S. and Karim, M.R. 2010. Fabrication and characterization of poly(vinyl alcohol)/alginate blend nanofibers by electrospinning method. Colloids and Surfaces A: Physicochemical and Engineering Aspects. 366(1-3), 135-140.
- Jadbabaei, S., Kolahdoozan, M., Naeimi, F. and Ebadi-Dehaghani, H. 2021. Preparation and characterization of sodium alginate-PVA polymeric scaffolds by electrospinning method for skin tissue engineering applications. RSC Advances. 11(49), 30674.
- Joy, N., Anuraj, R., Viravalli, A., Dixit, H.N. and Samavedi, S. 2021. Coupling between voltage and tip-to-collector distance in polymer electrospinning: Insights from analysis of regimes, transitions and cone/jet features. Chemical Engineering Science, 230, 116200.
- Kahya, N. and Gürarslan, A. 2025. Preparation and characterization of wet-spun porous calcium alginate fibers. Journal of the Textile Institute. Preprint.
- Kenawy, E.R.S., Kamoun, E.A., Eldin, M.S., Soliman, H.M.A., EL-Moslamy, S.H., El-Fakharany, E.M. and Shokr, A.-b.M. 2023. Electrospun PVA-dextran nanofibrous scaffolds for acceleration of topical wound healing: Nanofiber optimization, characterization and in vitro assessment. Arabian Journal for Science and Engineering. 48(1), 205-222.
- Khalaji, S., Golshan Ebrahimi, N. and Hosseinkhani, H. 2021. Enhancement of biocompatibility of PVA/HTCC blend polymer with collagen for skin care application. International Journal of Polymeric Materials and Polymeric Bio-materials. 70(7), 459-468.
- Khalili, A.A. and Ahmad, M.R. 2015. A review of cell adhesion studies for biomedical and biological applications. International Journal of Molecular Sciences. 16(8), 18149.
- Kinler, Z.E., Davis, A., Spiva, J.A., Hamilton, S.K., Rezoagli, E., Murphy, E., Major, I., Penton, K.E., Kinler, Z., Davis, Amber, Spiva, J.A. and Hamilton, Sharon K. 2022. Electrospinning

- drug-loaded alginate-based nanofibers towards developing a drug release rate catalog. Polymers. 20(14), 2773.
- Li, J., Wu, Y., He, J. and Huang, Y. 2016. A new insight to the effect of calcium concentration on gelation process and physical properties of alginate films. Journal of Materials Science. 51(12), 5791-5801.
- Li, Y., Zhu, J., Cheng, H., Li, G., Cho, H., Jiang, M., Gao, Q. and Zhang, X. 2021. Developments of advanced electrospinning techniques: A critical review. Advanced Materials Technologies. 6(11), 2100410.
- Majidi, S.S., Slemming-Adamsen, P., Hanif, M., Zhang, Z., Wang, Z. and Chen, M. 2018. Wet electrospun alginate/gelatin hydrogel nanofibers for 3D cell culture. International Journal of Biological Macromolecules. 118, 1648-1654.
- Mata, G.C. da, Morais, M.S., Oliveira, W.P. de and Aguiar, M.L. 2022. Composition effects on the morphology of PVA/chitosan electrospun nanofibers. Polymers. 14(22), 4856.
- Meng, Q., Li, Y., Wang, Q., Wang, Y., Li, K., Chen, S., Ling, P. and Wu, S. 2024. Recent advances of electrospun nano-fiber-enhanced hydrogel composite scaffolds in tissue engineering. Journal of Manufacturing Processes. 123, 112-127.
- Miranda, C.S., Silva, A.F.G., Pereira-Lima, S.M.M.A., Costa, S.P.G., Homem, N.C. and Felgueiras, H.P. 2022. Tunable spun fiber constructs in biomedicine: Influence of processing parameters in the fibers' Architecture. Phar-maceutics. 14(1), 164
- Mohammadalizadeh, Z., Bahremandi-Toloue, E. and Karbasi, S. 2022. Recent advances in modification strategies of pre- and post-electrospinning of nanofiber scaffolds in tissue engineering. Reactive and Functional Polymers. 172, 105202.
- Mohammadi, S., Ramakrishna, S., Laurent, S., Shokrgozar, M.A., Semnani, D., Sadeghi, D., Bonakdar, S. and Akbari, M. 2019. Fabrication of nanofibrous PVA/alginate-sulfate substrates for growth factor delivery. Journal of Biomedical Materials Research Part A. 107(2), 403-413.
- Nie, H., He, A., Zheng, J., Xu, S., Li, J. and Han, C.C. 2008. Effects of chain conformation and entanglement on the electrospinning of pure alginate. Biomacromolecules. 9(5), 1362-1365.
- Nista, S.V.G., Bettini, J. and Mei, L.H.I. 2015. Coaxial nanofibers of chitosan-alginate-PEO polycomplex obtained by electrospinning. Carbohydrate Polymers. 127, 222-228.
- Qin, X. 2017. Coaxial electrospinning of nanofibers. Electrospun Nanofibers. 41-71.
- Rathee, S., Singh, K.R., Mallick, S., Singh, J., Pandey, S.S., Ojha, A. and Singh, R.P. 2024. Smart alginate nanomaterials: Revolutionizing food across delivery, preservation, packaging, safety, and waste upcycling. Carbohydrate Polymer Technologies and Applications. 8, 100568.
- Riss, T.L., Moravec, R.A., Niles, A.L., Duellman, S., Benink, H.A., Worzella, T.J. and Minor, L. 2016. Cell viability assays. Assay Guidance Manual.
- Sadeghi-Aghbash, M., Rahimnejad, M., Adeli, H. and Feizi, F. 2022. Fabrication and development of PVA/Alginate nanofibrous mats containing *Arnebia euchroma* extract as a burn wound dressing. Reactive and Functional Polymers. 181, 105440.
- Safi, S., Morshed, M., Ravandi, S.A.H. and Ghiaci, M. 2007. Study of electrospinning of sodium alginate, blended solutions of sodium alginate/poly(vinyl alcohol) and sodium alginate/ poly(ethylene oxide). Journal of Applied Polymer Science. 104(5), 3245-3255.

- Shalumon, K.T., Anulekha, K.H., Nair, Sreeja V., Nair, S. V., Chennazhi, K.P. and Jayakumar, R. 2011. Sodium alginate/ poly(vinyl alcohol)/nano ZnO composite nanofibers for antibacterial wound dressings. International Journal of Biological Macromolecules. 49(3), 247-254.
- Silva, T.N., Gonçalves, R.P., Rocha, C.L., Archanjo, B.S., Barboza, C.A.G., Pierre, M.B.R., Reynaud, F. and de Souza Picciani, P.H. 2019. Controlling burst effect with PLA/PVA coaxial electrospun scaffolds loaded with BMP-2 for bone guided regeneration. Materials Science and Engineering: C. 97, 602-612.
- Singaravelu, S., Madhan, B., Abrahamse, H. and Dhilip Kumar, S.S. 2024. Multifunctional embelin- poly (3-hydroxybutyric acid) and sodium alginate-based core-shell electrospun nanofibrous mat for wound healing applications. International Journal of Biological Macromolecules. 265, 131128.
- Sreedhar, S., Illyaskutty, N., Sreedhanya, S., Philip, R. and Muneera, C.I. 2016. An organic dye-polymer (phenol red-poly (vinyl alcohol)) composite architecture towards tunable-optical and -saturable absorption characteristics. Journal of Applied Physics. 119(19), 193106.
- Suresh, S., Becker, A. and Glasmacher, B. 2020. Impact of apparatus orientation and gravity in electrospinning—A review of empirical evidence. Polymers Basel. 12, 2448.
- Taemeh, M.A., Shiravandi, A., Korayem, M.A. and Daemi, H. 2020. Fabrication challenges and trends in biomedical applications of alginate electrospun nanofibers. Carbohydrate Polymers. 228, 115419.
- Tang, Y., Lan, X., Liang, C., Zhong, Z., Xie, R., Zhou, Y., Miao, X., Wang, H. and Wang, W. 2019. Honey loaded alginate/PVA nanofibrous membrane as potential bioactive wound dressing. Carbohydrate Polymers. 219(May), 113-120.
- Türkoğlu, G.C., Khomarloo, N., Mohsenzadeh, E., Gospodinova, D.N., Neznakomova, M. and Salaün, F. 2024. PVA-based electrospun materials—A promising route to designing nanofiber mats with desired morphological shape—A review. International Journal of Molecular Sciences. 25(3), 1668.
- Wang, F., Hu, S., Jia, Q. and Zhang, L. 2020. Advances in electrospinning of natural biomaterials for wound dressing. Journal of Nanomaterials. https://doi.org/10.1155/2020/8719859
- Wang, M. and Zhao, Q. 2019. Electrospinning and electrospray for biomedical applications, Encyclopedia of Biomedical Engineering. Elsevier Inc.
- Wang, X., Ding, B. and Li, B. 2013. Biomimetic electrospun nanofibrous structures for tissue engineering. Materials Today. 16(6), 229-241.
- Wang, X. and Nakane, K. 2020. Preparation of polymeric nanofibers via immersion electrospinning. European Polymer Journal. 134, 109837.
- Wu, J., Yu, F., Shao, M., Zhang, T., Lu, W., Chen, X., Wang, Y. and Guo, Y. 2024. Electrospun nanofiber scaffold for skin tissue engineering: A review. ACS Applied Bio Materials. 7(6), 3556-3567.
- Xue, J., Wu, T., Dai, Y. and Xia, Y. 2019. Electrospinning and electrospun nanofibers: Methods, materials, and applications. Chemical Reviews. 119(8), 5298-5415.

